

The transverse momentum of Z^0 in $p\bar{p}$ collisions at CDF, the associated Γ_W uncertainty, and next-to-leading-order QCD corrections to W production

First Year Transfer Report

Daniel Beecher
Department of Physics and Astronomy
University College London

Summer 2006

Abstract

The transverse momentum distribution of Z bosons was investigated and modelled using a four-parameter functional form. Best fits to the data were made with χ^2/dof of 0.982 and 1.429 for $Z^0 \rightarrow ee$ and $Z^0 \rightarrow \mu\mu$ respectively, indicating that the electrons can be well described by the fast simulation used by there is work to be done to understand the muon data. The effect of uncertainty in the $p_T(Z)$ fits upon the Γ_W was also investigated and was found to introduce a 5.252 MeV and 5.398 MeV systematic uncertainty for $W \rightarrow e\nu_e$ and $W \rightarrow \mu\nu_\mu$.

The shift in U_{\parallel} from including next-to-leading order QCD corrections has been estimated to be +8.6 MeV and +9.6 MeV for $W \rightarrow e\nu_e$ and $W \rightarrow \mu\nu_\mu$ respectively.

Contents

1	Introduction	3
1.1	The Standard Model	3
1.2	Glashow–Weinberg–Salam Model	3
2	CDF	4
2.1	Tevatron	4
2.2	CDF detector	4
3	Physics motivation	4
3.1	W Boson Width	4
3.2	Kinematics	5
3.2.1	Transverse plane	6
3.2.2	Transverse momentum	6
3.2.3	Boson recoil and U_{\parallel}	6
4	CDF fast simulation	6
5	Z boson transverse momentum	7
5.1	Modeling Z transverse momentum in UCL fast simulation	7
5.2	Determining effect upon $\Delta\Gamma_W$	9
6	Next-to-leading order QCD polarisation corrections	10
6.1	Helicity corrections to tree-level QCD	10
6.2	The Collins–Soper frame	11
6.3	Modelling NLO QCD in UCL fast simulation	12
7	Conclusions and Future Work	12

1 Introduction

1.1 The Standard Model

It has long been recognised that there are four fundamental forces dictating the behaviour of particles in the universe. The ancients recognised these forces as earth, air, fire, and water; science has progressed over the centuries and modern physicists have a new quartet: the electromagnetic force, the weak force, the strong force, and gravity. While the ability to unite these lies beyond the current reach of physics, the interactions of particles via the first three forces can be understood in terms of the Standard Model.¹

The Standard Model traces its roots back to the developments in particle physics during the late 1970s in the search for a Grand Unified Theory of particle interactions. It consists of two principal theories: the Glashow–Weinberg–Salam (GWS) model of electroweak interactions and Quantum Chromodynamics (QCD) governing the strong force and interactions between quarks.

1.2 Glashow–Weinberg–Salam Model

In the 1960s, Sheldon Glashow, Mark Weinberg, and Albus Salam developed a model of the weak interaction whereby the weak charged interaction is interpreted as the coupling of left-handed doublets in weak-isospin space governed by the $SU(2)_L$ symmetry group. The neutral current is similar but with additional right-handed weak iso-singlets states, requiring that the symmetry group be enlarged to the $SU(2)_L \otimes U(1)_Y$ weak isospin-hypercharge symmetry group.

One success of the GWS model is the unification of the weak and electromagnetic interactions. The generators of the governing $SU(2)_L \otimes U(1)_Y$ symmetry group are W_μ^1 , W_μ^2 , W_μ^3 , and B_μ , which form the massless electroweak gauge bosons at energy above that of the electroweak symmetry breaking scale. At lower energies the $W_\mu^{1,2}$ are recognised as the massive W^\pm and the remaining massless boson mix to reveal the massless photon and massive neutral weak boson, (1.1).

$$\begin{aligned} A_\mu &= B_\mu \cos \theta_W + W_\mu^3 \sin \theta_W \\ Z_\mu &= -B_\mu \sin \theta_W + W_\mu^3 \cos \theta_W \end{aligned} \tag{1.1}$$

$$\rho = \frac{M_W^2}{M_Z^2 \cos^2 \theta_W} \tag{1.2}$$

The Weinberg mixing angle, θ_W , can also be shown to relate the masses of the weak bosons (1.2) where ρ is preferred to be unity for theoretical reasons.² This is in good agreement with the current estimate of $\rho = 1.01$ given $M_W = 80.425 \pm 0.038$ GeV, $M_Z = 91.1876 \pm 0.0023$ GeV and $\sin^2 \theta_W = 0.23120 \pm 0.00015$. [6]

¹The situation is not ideal but the lack of gravity is not damaging to the credibility of the Standard Model. While gravity dominates everyday life it is a relatively tiny force in comparison with the other three and can be neglected at current energy scales.

²The massive nature of the weak bosons is incompatible with the concept of local gauge invariance where the interacting gauge fields must be massless. This is saved for the weak interaction by including an additional complex doublet of fields in weak isospin. The most economical choice of field, the Weinberg-Salam Higgs model predicts $\rho = 1$.

2 CDF

2.1 Tevatron

The Tevatron is a particle accelerator at the Fermi National Accelerator Laboratory at Batavia, Illinois and it is currently the world's highest energy collider in operation.³ It accelerates bunches of protons and anti-protons and with the upgrade to Run-II in recent years the Tevatron now collides these bunches with a 1.96 TeV centre-of-mass energy for use in experiments such as CDF and D0. A stated goal is to produce 15 fb^{-1} of data at this energy from CDF and D0 in the operational lifetime of the accelerator.

2.2 CDF detector

The Collider Detector at Fermilab (CDF) [4] is a general purpose detector that has been in operation since 1985. Along with D0 it discovered the top quark in 1994 and has the most precise measurement of its mass to date. The detector was upgraded at the same time as the Tevatron.

CDF uses cylindrical coordinates defined so that the polar angle, θ , is measured from the incoming proton, and the azimuthal angle, ϕ , is measured from the Tevatron plane.

Immediately surrounding the beam-pipe in the central barrel region is the first of the tracking systems, the Silicon Vertex Tracker (SVX) covering $|\eta| \leq 2$. The Immediate Silicon Layer (ISL) covers a $|\eta| \leq 1.9$ and in conjunction with the SVX is designed for precise tracking and b-quark tagging. The Central Outer Tracker (COT) covers $|\eta| \leq 1$ in the barrel region. The 1.4 T solenoid surrounds the tracking systems before the calorimetry.

The calorimetry systems cover $|\eta| \leq 3$ in the barrel and plug regions and consist of dedicated electromagnetic (CEM and PEM) and hadron (CHA and PHA) sampling calorimeters.

The yoke for the solenoid provides part of the absorbing material for the muon tracking systems surrounding the calorimeters.

3 Physics motivation

3.1 W Boson Width

The work in this document is intended to aid in a precise and accurate measurement of the width of the W^\pm . At lowest order in perturbation theory, the partial decay width of the W boson according to the Standard Model is: [6]:

$$\Gamma(W^+ \rightarrow e^+ \nu_e) = \frac{G_F M_W^3}{6\pi\sqrt{2}} \approx 226.56 \pm 0.24 \text{ MeV} \quad (3.1a)$$

$$\Gamma(W^+ \rightarrow q_i \bar{q}_j) = \frac{CG_F M_W^3}{6\pi\sqrt{2}} |V_{ij}|^2 \approx (707.1 \pm 0.7) |V_{ij}|^2 \text{ MeV} \quad (3.1b)$$

$G_F = \frac{\sqrt{2}g_W^2}{8M_W^2 c^4}$ is Fermi's constant⁴ and is the coupling strength of Fermi's point-like weak interaction in his theory of beta decay; C is the colour factor where $C = 3(1 + \text{QCD corrections})$

³The Tevatron is set to be supplanted as the highest-energy collider when the Large Hadron Collider begins taking data in 2007.

⁴Natural units, i.e. $c = \hbar = 1$, are to be used throughout this document

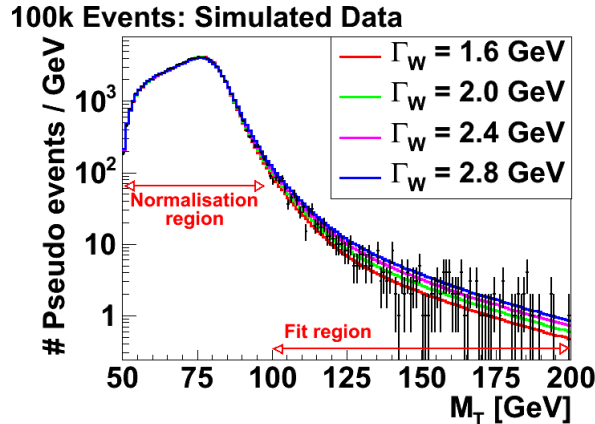


Figure 1: Γ_W is determined by fitting simulated M_T line-shapes to M_T data. The majority of the events are used to normalise the line-shapes to the data and the small tail is the region of M_T over which the fit is made.

for quarks; V_{ij} is the Cabbibo–Kobayashi–Maskawa (CKM) matrix indicating the the quark mixing content of the weak interaction. The Standard Model prediction of the full width is $\Gamma_W \approx 2.0936 \pm 0.0022$ GeV and compares well with measurement, $\Gamma_W = 2.124 \pm 0.041$ GeV [6].

Reducing the uncertainty in the measurement of Γ_W will show if there is any discrepancy between the Standard Model and reality, indicating new physics in this area.

The method of measuring Γ_W will be to understand and accurately model the underlying physical processes in order to simulate W^\pm transverse mass, M_T^W , line-shapes for a range of Γ_W from Monte Carlo, then fitted to data as the example fits in Figure 1 show.

3.2 Kinematics

The Tevatron’s collisions of interest are principally Drell–Yan processes the collision of two hadrons which contain several underlying event processes which need to be understood.

Hard $q\bar{q}$ interaction: The principle sub-event of interest is that of the $q\bar{q}$ from the colliding $p\bar{p}$ pair. Characteristic features of the hard interaction are jets with high transverse momenta from the decay of weak intermediate vector bosons.

Initial and final state radiation: The incoming partons in a Drell-Yan event can radiate photons if charged via Bremsstrahlung, and are liable to radiating gluons which can lead to unwelcome uncertainty in the properties of the hard sub-event. Further radiation can occur from the primary vertex before detection.

Underlying soft interaction: The remnants of the colliding hadrons will also interact giving a minimum bias event—an event that passes minimal cuts for detection—or a zero bias event—and event that fails to pass any cuts.

This demarcation is somewhat arbitrary but it aids in understanding the Monte Carlo event generation process covered in §4.

3.2.1 Transverse plane

The technical constraints of detector building inevitably leave particle detectors having low resolution in the longitudinal direction. It is for this reason that it is more appropriate to work and measure properties transverse to the the beam pipe, the transverse plane.

$$E_T^2 = p_T^2 + M_T^2 = (p_T^l + p_T^{\nu_l})^2 + (m_T^l)^2 \quad (3.2)$$

3.2.2 Transverse momentum

At greater centre-of-mass energies higher-order corrections to the $q\bar{q}$ collisions start to become significant for larger amounts of pre-collision radiation leads to the vector bosons being produced with non-zero transverse momenta.

For the decay of Z^0 this can be reconstructed from the transverse momenta of the leptonic decay products. The uncertainty in the transverse momentum of the W^\pm is more difficult to reconstruct given the evasive nature of the resulting neutrino and the information lost as a result.

3.2.3 Boson recoil and U_\parallel

It is important to have an understanding of the missing energy and momenta of the neutrinos in order to understand the uncertainty in the M_T^W line-shapes. The total angular momenta in the event will be conserved and as such the transverse momentum of the boson can be determined by measuring the rest of the event that recoils against it, the boson recoil, \vec{U} . It is defined as the sum of all the energies in those towers where energy was not deposited by the lepton produced in the boson decay, (3.3).

$$\vec{U} = \sum_i (E_i \sin \theta_i) \hat{n}_i \quad (3.3)$$

θ_i is the i th tower's polar angle and \hat{n}_i is the vector pointing from the vertex to the tower. It is usually decomposed into the parallel and perpendicular components, U_\parallel and U_\perp , of which U_\parallel is the greater contributor to the uncertainty in the missing E_T .

$$U_\parallel = \frac{\vec{U} \cdot \vec{E}_T}{E_T} \quad U_\perp = \frac{|\vec{U} \times \vec{E}_T|}{E_T} \quad (3.4)$$

An accurate boson recoil model is essential in order to reconstruct the missing neutrino energy and momentum.

$$p_T^{\nu_l} = -\vec{U} - p_T^l \quad (3.5)$$

4 CDF fast simulation

The Monte Carlo used was TOYGEN, a FORTRAN program originally written by Michel Lefebvre so simulate first-order Drell-Yan processes decaying into a leptonic pair of the user's choice. The simulation reproduced the aforementioned sub-events as follows:

Hard $q\bar{q}$ interaction: TOYGEN generates two random variables according to the incoming quark PDFs and creates the boson 4-momentum at rest from the incoming parton 4-momenta using a generic $q\bar{q} \rightarrow X$. The particular flavours involved are randomly generated and the

event is ascribed the associated weight. The vector boson is boosted into the lab frame by a random transverse momentum which is covered in more detail in §5.1. The 4-momenta of the resulting leptons is then shared equally in a back-to-back decay, with the angle of the primary lepton randomly generated and the angular weight added to the event.

Initial state radiation: The effect of QED radiation prior to interaction can be included with the use of radiative corrections by Berends *et al* [3]. QCD radiation corrections are not calculated and are built into the transverse momentum ascribed to the the boson.

Final state radiation: Radiative QED corrections can be implemented using Berends or from the PHOTOS package [2] inside TOYGEN. The simulation of the detector can account for energy lost by the leptons via Bremsstrahlung passing through the silicon layers of the detector; ionization energy losses are also simulated. As of yet the effects of the COT and solenoid have not been built into the simulation.

Underlying event: This is not simulated.

5 Z boson transverse momentum

5.1 Modeling Z transverse momentum in UCL fast simulation

The transverse momentum of the Z^0 could have been estimated in a number of ways. One such way was using a generator like RESBOS (The Monte Carlo for Re-summed Boson Production and Decay) which can evaluate the QCD effects unlike the more light-weight TOYGEN. However, RESBOS evades the problem of the non-perturbative nature of the low p_T QCD by using fits to data in the long-distance QCD interaction limit. It is unfortunate that the peak of the $p_T(Z)$ distribution is found in this region. Considering that the peak of the distribution was derived in some part from fits to Run-I data [1] it was deemed more time efficient to fit an arbitrary functional form to data as a means of determining $p_T(Z)$ for Z^0 . The same functional form, (5.1), as used in Run-I [8] was chosen for this analysis.

$$\frac{d\sigma}{dp_T} = \frac{\left(\frac{p_T}{50}\right)^{P_4}}{\Gamma(P_4 + 1)} (1 - P_1) P_2^{P_4+1} e^{-\frac{P_2 p_T}{50}} P_1 P_3^{P_4+1} e^{-\frac{P_3 p_T}{50}} \quad (5.1)$$

The p_T of the boson is then determined by randomly generating a transverse momentum for the boson and re-weighting the event according to (5.1). This P_T is then reweighted to be a $p_T(W)$ if needed.

With a parametrisation of $p_T(Z)$ the effect of the CDF resolution upon the distributions needed to be taken into account before fitting to data.

UCL's fast simulation of the CDF was used to generate a list of several million transverse momenta pairs: the true transverse momentum, p_T^T of the Z^0 inside the detector, and the quantity that is reconstructed, p_T^M . This data allowed the re-weighting of any line-shape generated by an arbitrary choice of P_1 - P_4 from (5.1) into the line-shape as would be seen if it were reconstructed from data so that this $p_T(Z)$ distribution could be fitted to data. A matrix method was chosen as the method of re-weighting.

P_i	$Z^0 \rightarrow ee$	$Z^0 \rightarrow \mu\mu$
P_1	0.623916 ± 0.00326841	0.586342 ± 0.00162309
P_2	4.38931 ± 0.0432713	5.18303 ± 0.0200603
P_3	15.2250 ± 1.50293	16.4733 ± 0.0896764
P_4	0.759204 ± 0.00918091	0.973354 ± 0.00721024

Table 1: The parameters for the best fits of (5.1) to $Z^0 \rightarrow ee$ and $Z^0 \rightarrow \mu\mu$ data with the parabolic error quoted.

Each of the transverse momentum distributions generated from the fast simulation were essentially $1 \times N$ vectors with each element corresponding to the number of events in each bin. Therefore it could be assumed that there exists a $N \times N$ matrix that transforms the p_T^T into the p_T^M

$$\begin{pmatrix} p_0^M \\ p_1^M \\ \vdots \\ p_n^M \end{pmatrix} = \begin{pmatrix} m_{00} & m_{01} & \dots & m_{0n} \\ m_{10} & m_{11} & \dots & m_{1n} \\ \vdots & \vdots & \ddots & \vdots \\ m_{n0} & m_{n1} & \dots & m_{nn} \end{pmatrix} \begin{pmatrix} p_0^T \\ p_1^T \\ \vdots \\ p_n^T \end{pmatrix} \quad (5.2)$$

This matrix was created by binning the weight of each pseudo-event into m_{ji} where the transverse momenta pair were placed into the i th p_T^T and the j th p_T^M bins. The matrix was normalised by insisting $\sum_{i=1}^N m_{ji} = 1$.

The validity of the method was checked by using the Monte Carlo to create a generator level $p_T(Z)$, p_T^T , the simulated $p_T(Z)$, p_T^M and the associated smearing matrix from 150 million pseudo-events. The smearing matrix created was used with the true $p_T(Z)$ and compared with the simulated $p_T(Z)$, both normalised to 8000, the same order of events as in the data. The χ^2 for the $Z^0 \rightarrow ee$ simulation was 0.235 for 50 degrees of freedom and the χ^2 for the $Z^0 \rightarrow \mu\mu$ simulation was 0.362 for 50 degrees of freedom.

In order to ensure that the pseudo-data samples were trustworthy and not sensitive to statistical fluctuations, fifty 10k pseudo-event samples were generated and the best fit functional form found for both the $Z^0 \rightarrow ee$ and $Z^0 \rightarrow \mu\mu$ simulations. A Gaussian distribution was fit to the range of χ^2 to find σ_{10k} . Asserting that the sample was not subject to statistical fluctuations if $\sigma_N \equiv \sigma_{\chi^2} \leq 1$, then the number of events required is found considering $\sigma_N = \sqrt{\frac{N}{n}} \sigma_n$.

Before cuts, 13 million pseudo $Z^0 \rightarrow ee$ and 18 million $Z^0 \rightarrow \mu\mu$ decays were deemed to be a large enough number so as to be unaffected by statistical fluctuations; 150 million simulated $Z^0 \rightarrow ee$ and $Z^0 \rightarrow \mu\mu$ events were used to create electron and muons smearing matrices and, in conjunction with (5.1), fitted to Run-II data with Minuit, yielding the parameters in Table 1.⁵ The $p_T(Z)$ generating aspect of TOYGEN was updated with the new parameters and the fast simulation was used to create 150 million pseudo-events. Figure 2 shows the comparison between the reconstructed data and the simulation. The simulation of the $Z^0 \rightarrow ee$ compares satisfactorily with the reconstructed data, Figure 2(a), the χ^2 of 49.1 for 50 degrees of freedom shows that the Run-I functional form does still describe the Run-IIb data without needing further modification. However, as Figure 2(b) shows, the $Z^0 \rightarrow \mu\mu$ simulation does not compare as well with data the electrons, the χ^2 being 71.5 for 50 degrees of freedom. There is a large disagreement between

⁵The errors from the fit were asymmetric but the parabolic errors are those that go into the covariance matrix which is sampled to find the effect of the $p_T(Z)$ fits on the Γ_W measurement.

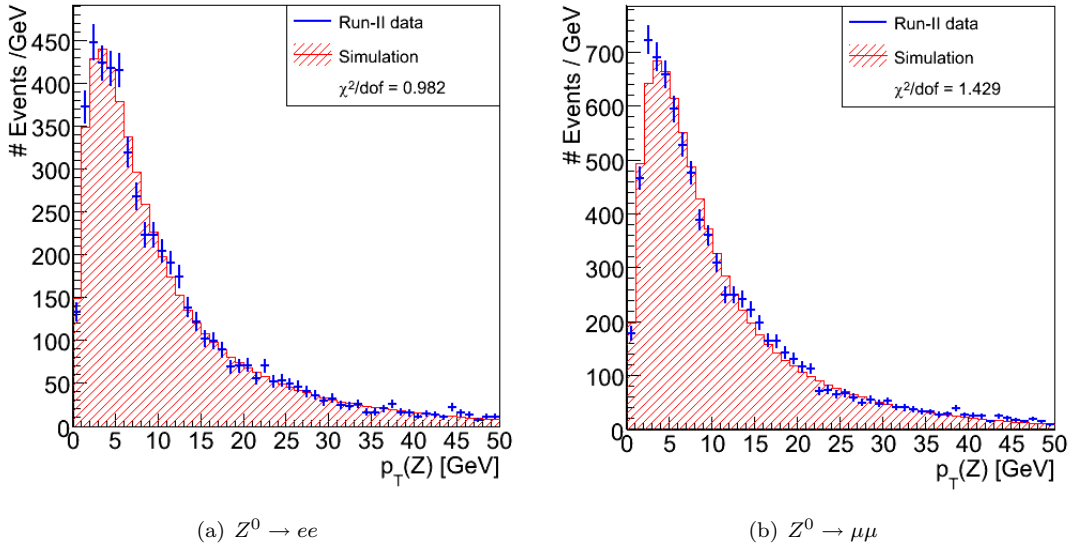


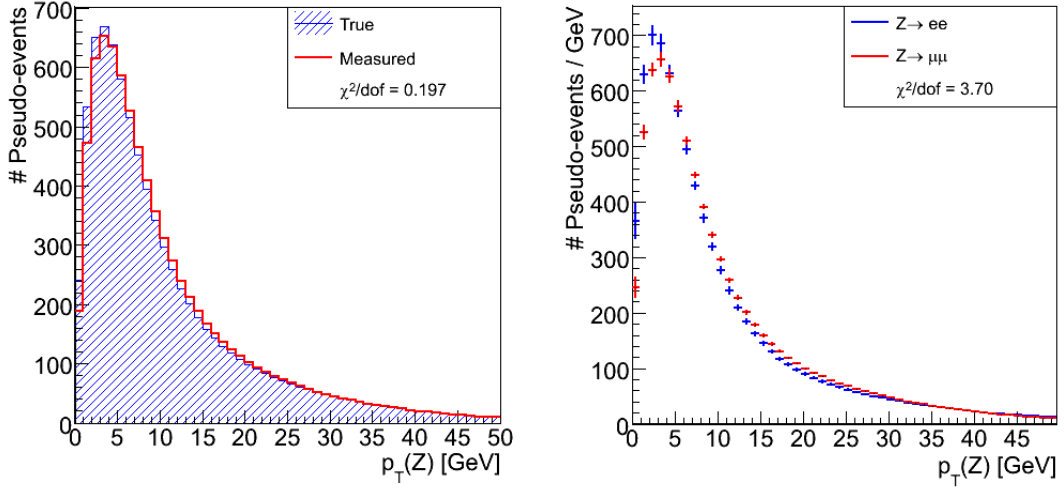
Figure 2: The $p_T(Z)$ distribution for $Z^0 \rightarrow ee$ and $Z^0 \rightarrow \mu\mu$ after the best fit parameters in Table 1 were put into TOYGEN and the simulation run for 150 million events.

the simulation and data in the 3 GeV region which the functional form is unable to reproduce. The effect of the detector simulation upon the generator level $p_T(Z)$ distribution is minor when compared with the comparison between the generator level $p_T(Z)$ distributions. There is no *a priori* reason why the $p_T(Z)$ distribution of electrons and muons should disagree to such an extent, it may be more likely that the functional form is unable to describe the muon data if there are still backgrounds in the data.

5.2 Determining effect upon $\Delta\Gamma_W$

The statistical uncertainty of the estimated $p_T(Z)$ for the Z^0 —and thus that of the W^\pm —manifests as a systematic error on the predicted value of Γ_W from the fast simulation. This uncertainty was estimated by using the covariance matrix of the $p_T(Z)$ fit to generate 250 alternative $p_T(Z)$ line-shapes within 1σ with which to re-weight pseudo-events. For every event generated the transverse mass of the W boson was re-weighted according to each of the 250 alternative $p_T(Z)$ line-shapes, and then re-weighted over a range of Γ_W .

A 30 million pseudo-event sample was generated and each of the 250 ‘pseudo-experiments’ produced an array of transverse mass histograms for different values of Γ_W ; these were fitted against an unweighted transverse mass sample to produce 250 different measurements of Γ_W ; 496,194 pseudo-events passed the cuts for $W \rightarrow e\nu_e$ simulation and 323,394 $W \rightarrow \mu\nu_\mu$ pseudo-event passed cuts. Gaussian fits to these spreads of Γ_W values gave $\Delta\Gamma_W$ for $W \rightarrow e\nu_e$ and $W \rightarrow \mu\nu_\mu$. The statistical uncertainty on the mean of the fits was estimated by splitting the unweighted pseudo-data sample into 10k sub-samples and fitting each of these to the same M_T template and propagating this error to the full sample. It should be noted that the relatively few sub-samples, 48 and 32 respectively, makes the Gaussian assumption untrustworthy and the figures have been included to offer some perspective if the fitted mean Γ_W is to be compared with the expected 2.09 GeV. Table 2 shows that, in the $W \rightarrow e\nu_e$ simulation, the systematic uncertainty



(a) $Z^0 \rightarrow \mu\mu$ generator and detector level $p_T(Z)$ (b) Generator level $Z^0 \rightarrow ee$ and $Z^0 \rightarrow \mu\mu$ $p_T(Z)$

Figure 3: The disagreement between (b) the $Z^0 \rightarrow ee$ and $Z^0 \rightarrow \mu\mu$ generator level $p_T(Z)$ is greater than the disagreement the effect of (a) the detector resolution on the $p_T(Z)$.

Norm. range (GeV)	Fit range (GeV)	σ (MeV)	μ (GeV)
50–90	90–200	8.447 ± 0.463	$2.142 \pm 0.0005 \pm 0.0475$
50–95	95–200	7.063 ± 0.306	$2.103 \pm 0.0004 \pm 0.0491$
50–100	100–200	5.252 ± 0.243	$2.095 \pm 0.0003 \pm 0.0708$
50–105	105–200	3.886 ± 0.306	$2.086 \pm 0.0002 \pm 0.0569$
50–110	110–200	2.753 ± 0.127	$2.076 \pm 0.0001 \pm 0.1041$

Table 2: The Gaussian fit parameters to the spread of fitted Γ_W from $W \rightarrow e\nu_e$ pseudo-data. The mean is quoted with the error on the fit then the statistical error from the number of events passing cuts.

on Γ_W decreases as the more of the M_T distribution is used to normalise the data with less in the tail to fit against. The simulation indicates that this decreased uncertainty in Γ_W is offset by an increased statistical uncertainty.

6 Next-to-leading order QCD polarisation corrections

6.1 Helicity corrections to tree-level QCD

The leading-order and next-to-leading QCD corrections to the the W production cross-section (6.1) has a dependence on angular amplitudes coefficients, A_i and the polar and azimuthal angles in the Collins–Soper frame; the Standard Model predictions for the A_i amplitudes, Figure 4, have been extracted from the next-to-leading order DYRAD [7] generator for proton–anti-proton collisions producing W^+ events at $\sqrt{s} = 1.8$ TeV by Strologas and Errede. [9] In order to keep the definition of the Collins–Soper frame consistent for both W^- and W^+ bosons, amplitudes A_1 , A_4 , and A_6

Norm. range (GeV)	Fit range (GeV)	σ (MeV)	μ (GeV)
50–90	90–200	8.404 ± 0.387	$2.064 \pm 0.0005 \pm 0.0366$
50–95	95–200	6.841 ± 0.343	$2.051 \pm 0.0004 \pm 0.0446$
50–100	100–200	5.398 ± 0.288	$2.040 \pm 0.0003 \pm 0.0579$
50–105	105–200	3.727 ± 0.173	$2.058 \pm 0.0002 \pm 0.0665$
50–110	110–200	3.031 ± 0.145	$2.079 \pm 0.0002 \pm 0.0875$

Table 3: The Gaussian fit parameters to the spread of fitted Γ_W from $W \rightarrow \mu\nu_\mu$ pseudo-data. The mean is quoted with the error on the fit then the statistical error from the number of events passing cuts.

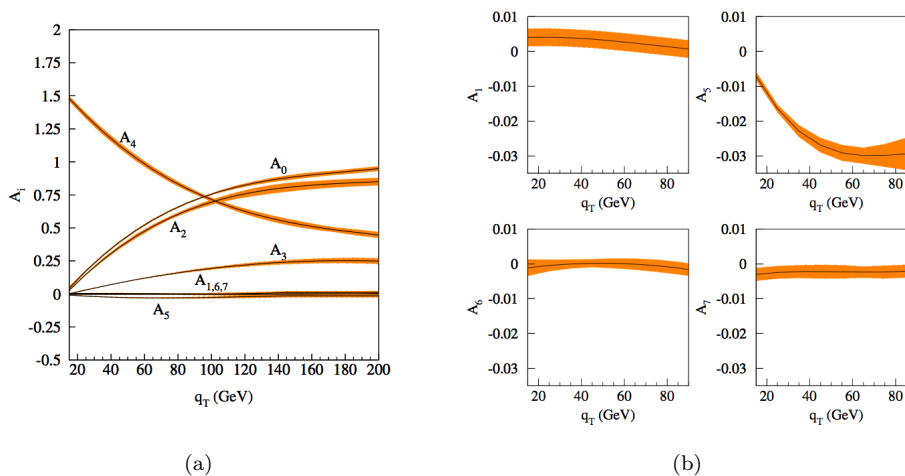


Figure 4: (a) The standard model prediction for the angular coefficients of the W produced at $\sqrt{s} = 1.8$ TeV. QCD effects are included up to order α_s^2 . The bands define the PDF and Q^2 systematics. (Credit: Figure 3 [9]) (b) The standard model prediction for the next-to-leading order coefficients (A_5 , A_6 , and A_7) and A_1 . (Credit: Figure 4 [9])

are inverted for the W^+ because $\theta \rightarrow \pi - \theta$ under the CP transformation.

$$\begin{aligned}
\frac{d\sigma}{dq_T^2 dy d\cos\theta_{CS} d\phi} &= \frac{3}{16\pi} \frac{d\sigma^\mu}{dq_T^2 dy} \left[(1 + \cos^2\theta_{CS}) + \frac{1}{2}A_0(1 - 3\cos^2\theta_{CS}) \right. \\
&+ A_1 \sin 2\theta_{CS} \cos\phi_{CS} + \frac{1}{2}A_2 \sin^2\theta_{CS} \cos 2\phi_{CS} + A_3 \sin\theta_{CS} \cos\phi_{CS} \\
&+ A_4 \cos\theta_{CS} + A_5 \sin^2\theta_{CS} \sin 2\phi_{CS} + A_6 \sin 2\theta_{CS} \sin\phi_{CS} \\
&\left. + A_7 \sin\theta_{CS} \sin\phi_{CS} \right] \quad (6.1)
\end{aligned}$$

6.2 The Collins–Soper frame

The Collins–Soper (CS) frame [5] is a particular orientation of the kinematics the rest frame of the boson. It is generated by defining \hat{z} as perpendicular to the transverse momentum of the boson then boosting into the boson rest frame. \hat{x} is defined as the unit vector bisecting the angle between the incoming proton and anti-proton. The \hat{x}, \hat{z} -plane is then rotated to be aligned with

the momenta of the the proton and anti-proton. θ_{CS} is then defined as the angle between the lepton and \hat{z} and ϕ_{CS} as the angle between the lepton and the \hat{x}, \hat{z} -plane. If there if the boson has no transverse momentum then the θ_{CS} is the same as θ in the lab frame and ϕ_{CS} is zero. Therefore, if a W^\pm is produced with no transverse momentum then the interaction is pure V–A and the only non-zero angular amplitude coefficient is A_4 , with the angular distribution the expected $(1 \pm \cos \theta)^2$. This is to be expected, the A_4 term comes from the V–A nature of the weak interaction: $(1 \pm \cos \theta)^2 = (1 + \cos^2 \theta) \pm 2 \cos \theta$.

6.3 Modelling NLO QCD in UCL fast simulation

The amplitude coefficients, Figure 4, were assumed to be linear for $0 \leq p_T \leq 50$ GeV and parametrised according to (6.2).

$$\begin{aligned} A_0 &= 0.01p_T & A_1 &= (0.005 - 0.00005p_T)\beta \\ A_2 &= A_1 & A_3 &= 0.0025p_T & \beta &= \begin{cases} +1 & W^- \\ -1 & W^+ \end{cases} \\ A_4 &= (2 - 0.01p_T)\beta & A_5 &= -0.006 - 0.00048p_T \\ A_6 &= 0 & A_7 &= -0.0002 \end{aligned} \quad (6.2)$$

The angular corrections were applied by defining a corrective multiplicative event weight while removing the pre-existing V–A angular weight, (6.3), where $f_i(\theta_{CS}, \phi_{CS})$ is the corresponding angular term in (6.2).

$$\frac{\sum_{i=0}^7 A_i f_i(\theta_{CS}, \phi_{CS})}{(1 + \beta \cos \theta_{lab})^2} \quad \beta = \begin{cases} +1 & W^- \\ -1 & W^+ \end{cases} \quad (6.3)$$

The effect of implementing the leading-order and next-to-leading-order corrections was to shift U_{\parallel} by +8.6 MeV for $W \rightarrow e\nu_e$ and by +9.6 MeV for $W \rightarrow \mu\nu_\mu$. No uncertainties from the A_i coefficients have been estimated as of yet.

7 Conclusions and Future Work

The fast simulation is able to describe the data for the $Z^0 \rightarrow ee$ decays but the disagreement between the $Z^0 \rightarrow ee$ and $Z^0 \rightarrow \mu\mu$ simulations needs to be understood. Considering the poor fit it may be that the Run-I functional form is not able to describe the Run-II muon data but it is also possible that there are backgrounds contaminating the sample.

The systematic effect of the uncertainty in the $p_T(Z)$ fits on Γ_W appears to be minor but the analysis should be redone with higher statistics to reduce the statistical uncertainty on the means of the Gaussian fits.

The shift in U_{\parallel} from the inclusion of the next-to-leading order QCD corrections by Strogas and Errede is small, +9 MeV, but the uncertainty in the Standard Model predictions should be included when a reliable estimate is found.

How the PDFs affect the $p_T(Z)$ fit and thus the Γ_W uncertainty is to be looked into in the future. Also, any bias coming in the $p_T(W)$ from the fast simulation’s implementation of the W cuts needs to be explored.

This work is designed to be used in a measurement of the W width and the potential thesis topic is a W mass measurement. The W mass measurement is often made using a fit M_T distribution

which is what is being modelling in this width analysis so this work will be needed to ensure that the statistical and systematic effects upon W mass are well understood.

References

- [1] C. Balazs and C. P. Yuan. Soft gluon effects on lepton pairs at hadron colliders. *Phys. Rev.*, D56:5558–5583, 1997.
- [2] E Barberio, B van Eijk, and Z Was. PHOTOS: A universal monte carlo for QED radiative corrections in decays. *Comput. Phys. Commun.*, 66:115–128, 1991.
- [3] F. A. Berends, R. Kleiss, J. P. Revol, and J. P. Vialle. QED radiative corrections and radiative decays of the intermediate weak bosons produced in proton - anti-proton collisions. *Z. Phys.*, C27:155, 1985.
- [4] R. Blair et al. The CDF-II detector: Technical design report. FERMILAB-PUB-96-390-E.
- [5] J. C. Collins and D. E. Soper. Angular distribution of dileptons in high-energy hadron collisions. *Phys. Rev.*, D16:2219, 1977.
- [6] S. Eidelman et al. Review of Particle Physics. *Physics Letters B*, 592:1+, 2004.
- [7] W. T. Giele and E. W. N. Glover. Higher order corrections to jet cross-sections in e^+e^- annihilation. *Phys. Rev.*, D46:1980–2010, 1992.
- [8] M. Lancaster and D. Waters. Vector boson p_T measurements. *J. Physics. G*, 26:646, 2000.
- [9] J. Strologas and S. Errede. Study of the angular coefficients and corresponding helicity cross sections of the W boson in hadron collisions. *Phys. Rev.*, D73:052001, 2006.